Proceedings of the ASME 2010 3rd Joint US-European Fluids Engineering Summer Meeting and 8th International Conference on Nanochannels, Microchannels, and Minichannels
FEDSM-ICNMM2010
August 1-5, 2010, Montreal, Canada

FEDSM-ICNMM2010-30799

FLOW AND HEAT TRANSFER OF NANOFLUIDS WITH TEMPERATURE DEPENDENT PROPERTIES

Ehsan Ebrahimnia Bajestan
Department of Mechanical Engineering, Faculty of Engineering, Ferdowsi University of Mashhad
Mashhad, Iran
Ehsan.Ebrahimnia@gmail.com

Hamid Niazmand
Department of Mechanical Engineering, Faculty of Engineering, Ferdowsi University of Mashhad
Mashhad, Iran
hniazmand@yahoo.com

Metin Renksizbulut
Mechanical & Mechatronics Engineering Department, University of Waterloo
Waterloo, Ontario, Canada, N2L 3G1

ABSTRACT

Numerical simulations of laminar convective heat transfer with nanofluids in two different geometries involving a straight pipe and a 90^o curved pipe are presented. The Navier-Stokes and energy equations for an incompressible Newtonian fluid are solved in a body fitted coordinate system using a control-volume method. In the present work, the nanofluid is a mixture of water and alumina particles, and its thermophysical properties are considered as a function of temperature as well as particle concentration. The accuracy of the models employed for estimating the effective thermophysical properties of this nanofluid are first evaluated using available experimental data for heat transfer in a straight pipe. The same models are then employed for the simulation of flows in a curved pipe.

Present results indicate that both the nanoparticle and curvature effects enhance the heat transfer performance but at the expense of increased pressure drop. However, in the present case, the nanoparticle contribution to the pressure drop is dominant, which increases by up to two orders of magnitude at higher nanoparticle concentrations. The ratio of the nanofluid Prandtl number to the based fluid Prandtl number is established as a criterion for the choice of a nanofluid. This ratio must be less than 1 to achieve higher heat transfer rates with relatively low pressure drops as the particle concentration is increased.

INTRODUCTION

Improvement in the performance of heat exchangers is a crucial need in a wide variety of industrial applications. The low thermal conductivities of conventional heat transfer fluids such as water, ethylene glycol and engine oil greatly limit the heat transfer performance of heat exchangers. One of the techniques to break this fundamental limit is suspending solid metal or metallic oxide particles into these conventional heat transfer fluids. Recent developments in nanotechnology lead to a new type of solid-fluid mixtures called nanofluids, which are suspensions of nanoparticles (less than 100 nm) in conventional fluids. Compared to millimeter or micrometer solid particle suspensions, nanofluids are very stable and almost free from problems of sedimentation, clogging, abrasion and erosion [1].

An important feature of nanofluids is thermal conductivity enhancement of the base fluid, which has been attributed to different parameters such as the volume fraction [2-9], size [2-7], shape [5 and 9] and type of the particle material [2,3,6], and to the temperature [3-5] and stability [7] of the nanofluid. Experimental data indicate that the convective heat transfer coefficients of nanofluids are also higher than those of the base fluids [10-15]. Besides the thermophysical properties of the base fluid that is influenced by the presence of the nanoparticles, other factors such as Brownian motion [13], particle–fluid interaction and particle migration [11] may also have an important role on the heat transfer performance of nanofluids.

The convective heat transfer characteristics of nanofluids have been studied for different sizes, type of materials and shapes of nanoparticles and flow conditions. Williams et al. [14] performed experiments on the turbulent heat transfer behavior of alumina (Al_2O_3) and zirconia (ZrO_2) inside a tube. They showed that the heat transfer and pressure-drop behavior of nanofluids under a fully developed turbulent flow matched with the correlations of a single-phase flow, if proper effective thermophysical properties are used in calculating the dimensionless numbers. Rea et al. [15] reported similar results on laminar flows of the same nanofluids.

There are some numerical studies simulating the convective heat transfer of various nanofluids such as TiO_2 [16], Al_2O_3

[17-21], CuO [18], Cu [18,22] and CNT [23] at different flow geometries such as straight tubes [16,18-20,22,23] and curved pipes [17,21], which appear in many industrial applications. Curved pipes enhance heat and mass transfer due to the generation of secondary flows. Despite the fact that there is a rich literature of fluid flow and heat transfer in curved tubes [24-28], the information available on convective heat transfer of nanofluids in curved pipes is rather limited. Akbarinia and Laur [17] and Akbarinia [21] have numerically studied the mixed convective heat transfer of Al_2O_3/water nanofluid in a 180° curved pipe.

The flow structure and heat transfer patterns in curved pipes are more complex than those in straight pipes. Previous studies indicate that curvature effects enhance the heat transfer rates; however, the effects of nanofluids have not been well documented. Therefore, in the present work, the effects of nanofluids on laminar convective heat transfer inside a 90 degree curved pipe have been studied. The incompressible Navier-Stokes and energy equations for Newtonian fluids are solved numerically in a body-fitted coordinate system using a control-volume technique. The effects of nanoparticles are considered by adopting the proper effective thermophysical properties reported in literature. The density and specific heat of the water mixture with nanoparticles are computed based on the classical two-phase mixture models. The effective thermal conductivity and the dynamic viscosity of nanofluids are obtained by available curve fits to experimental data reported in the literature. The thermophysical properties of nanofluids (density, viscosity, thermal conductivity, and specific heat) are considered as a function of temperature, in addition to the nanoparticle concentration. The numerical scheme with the effective thermophysical properties have been validated by the existing experimental data for straight pipes.

MATHEMATICAL MODELING

Figure 1 shows two pipes with the same length, L=1.01 m, and diameter, D=4.5mm. One is a straight pipe, while the other is a 90° curved circular pipe with two straight parts at both ends. The straight part at the curve inlet is 61D long, whereas it is extended to 91.25D at the curve exit to preserve the specified length and to ensure fully developed flow at the outlet of the flow domain. The curvature radius of the 90° bend is 46D as shown in Fig.1. This figure also includes the location of some selected cross sections and axial lines, which will be used to discussed the flow features later in the paper.

The governing equations for a laminar, incompressible, Newtonian flow are the Navier–Stokes and energy equations as follows:

$$\iint \rho_e \vec{V} \cdot d\vec{A} = 0 \tag{1}$$

$$\int_{\forall} \rho_e \frac{\partial \vec{V}}{\partial t} d\forall + \iint \vec{V} \rho_e \vec{V} \cdot d\vec{A} = -\iint P\vec{n} \cdot d\vec{A} + \iint \mu_e \vec{\nabla} \vec{V} \cdot d\vec{A} \tag{2}$$

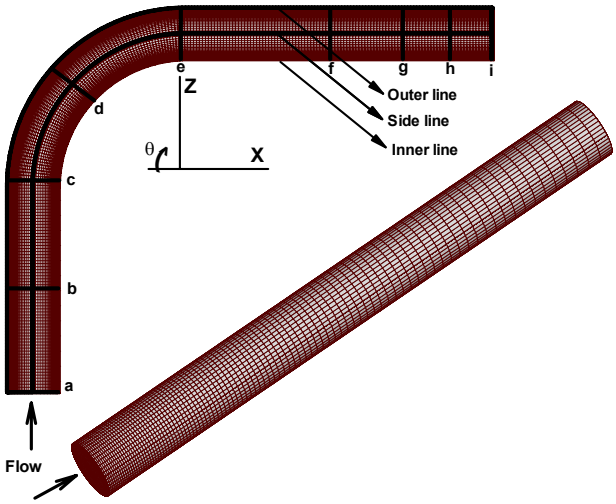

Figure 1. Flow geometries and the locations of the important cross sections and lines.

$$\int_{\forall} (\rho C_p)_e \frac{\partial T}{\partial t} d\forall + \iint (\rho C_p)_e T\vec{V} \cdot d\vec{A} = \iint k_e \vec{\nabla} T \cdot d\vec{A} \tag{3}$$

where $\vec{V}$, P and T are the velocity vector, pressure, and temperature. The effective thermophysical properties of the nanofluid indicated by the subscript e are density, ρ_e, thermal conductivity, k_e, dynamic viscosity, μ_e, and heat capacity, C_{p_e}. These effective properties are modeled as temperature dependent variables using available correlations and experimental data as follows:

Density:

$$\rho_e(\phi,T) = (1-\phi)\rho_f(T) + \phi\rho_p \tag{4}$$

Heat capacity:

$$C_{p_e}(\phi,T) = \frac{(1-\phi)\left(\rho(T)C_p(T)\right)_f + \phi(\rho C_p)_p}{(1-\phi)\rho_f(T) + \phi\rho_p} \tag{5}$$

The dynamic viscosity and thermal conductivity of Al_2O_3/water nanofluid as a function of temperature and nanoparticle volume fraction are taken from [15]:

$$\mu_e(\phi,T) = \mu_f(T)\exp\left[4.91\phi / (0.2092 - \phi)\right] \tag{6}$$

$$k_e(\phi,T) = k_f(T)(1 + 4.5503\phi) \tag{7}$$

As for boundary conditions, uniform velocity profile is assumed at the inlet, while zero gradients are applied to all variables at the outlet. At the walls, the no-slip condition for the velocity components and a constant heat flux for the thermal field are considered.

NUMERICAL METHOD

The numerical solution is based on a projection-type method which solves the flow field in two steps. First, an intermediate velocity field is obtained using the available pressure field. Next, velocity and pressure corrections are calculated from a Poison equation designed to satisfy the continuity equation. The numerical scheme was originally developed by Chorin [29] and improved further by Dwyer [30] and the present authors [31]. Following Dwyer et al. [28], a new pressure correction is employed to improve the convergence performance of the Poisson equation solver. The correction is based on the physical considerations of preserving mass flow rate at each cross section corresponding to the incompressible flow assumption. Therefore, the pressure correction, p', is obtained based on the local velocity defect as:

$$-\frac{\partial p'}{\partial s} = \rho \frac{\Delta U_k}{\Delta t} \tag{8}$$

where the local velocity defect, ΔU, at each cross section, k, is defined as:

$$\Delta U_k = U_i - \frac{\iint_A \vec{V} \cdot d\vec{A}}{A} \tag{9}$$

In the above equations, U_i is inlet velocity, s is the streamline direction, and A is pipe cross sectional area.

Extensive computations have been performed to identify the number of grid points that produces reasonably grid independent results. It was found that in the case of the curved pipe the minimum grid points of 42 × 41 × 251 are required in the azimuthal, radial, and axial directions, respectively. Uniform grid spacing is used in the azimuthal and axial directions, while the expansion ratio of 1.1 is employed in the radial direction.

VALIDATION

To validate the present numerical scheme, the results have been compared with the experimental data of [27] for steady flow in a 90° curved pipe with a curvature radius of 24mm and Reynolds number of 300 based on the pipe diameter of D = 8mm. The axial velocity profiles in the symmetric plane at several cross sections of the curve are compared with experimental data in Fig. 2, where reasonably good agreement is observed.

As for thermal validation of the model, the convective heat transfer of a nanofluid flow in a pipe has been considered. The numerical heat transfer coefficients have been compared with the experimental data of [15] for laminar flow in a straight pipe, 1.01m long and 4.5mm in diameter, under the constant heat flux condition. Experimentally, the applied heat flux is obtained by measuring the inlet and outlet temperature and the mass flow rate according to:

$$q_w = \frac{\dot{m} C_p \Delta T}{\pi D L} \tag{10}$$

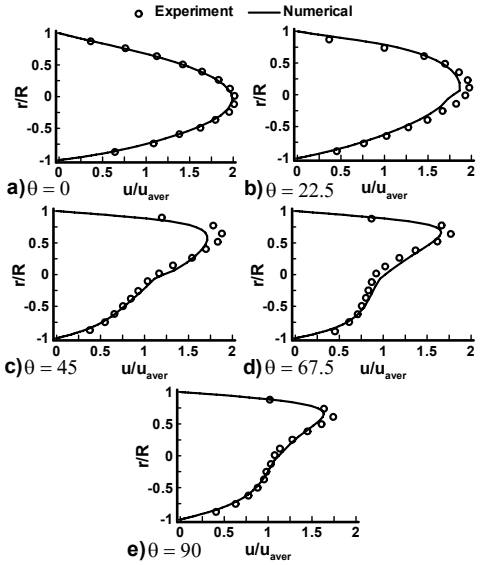

Figure 2. Comparison of axial velocity profiles with the experimental data [27] for flow in a 90° curved pipe.

The axial variations of the heat transfer coefficients for different Reynolds numbers and nanoparticle concentrations are compared with the experimental data in Fig. 3, where reasonably good agreement is observed.

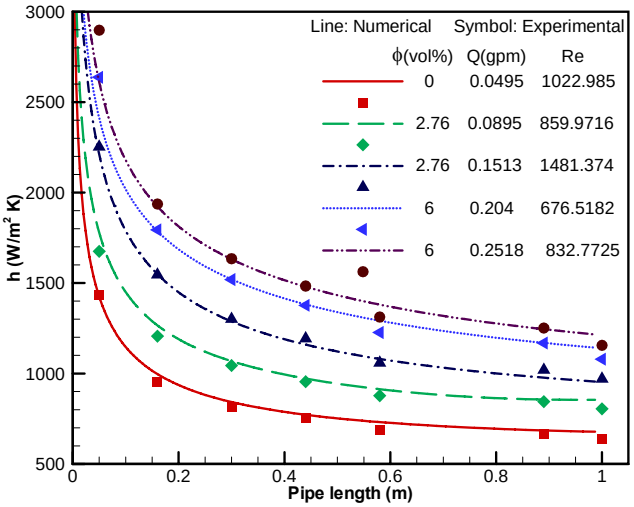

Figure 3. Comparison of the axial variations of the heat transfer coefficients (solid lines) with the experimental data (symbols) [15] for Al_2O_3/water nanofluid at different Re and nanoparticle concentrations.

RESULTS AND DISCUSSION

As mentioned earlier, the accuracy of the correlations developed for thermophysical properties of nanofluids can only be evaluated with the experimental data available for straight pipes (as in Fig. 3). However, not much information is available for the case of a curved pipe. Therefore, the same correlations have been employed for the numerical simulations of nanofluid

flow in a 90° curved pipe assuming that the thermophysical properties are basically independent of the flow geometry. The validity of this assumption still remains to be determined experimentally. The same length and diameter are chosen for straight and curved pipes, which makes the comparisons more convenient.

The results are presented for the Al_2O_3/water nanofluid similar to the case considered with respect to Fig. 3. The flow conditions of Re = 833, T_{inlet} = 25.6 °C, and a heat flux of q_w = 42316 W/m^2 are considered, which is basically one of the cases examined in the experimental study of [15] for a straight pipe. The axial variations of the heat transfer coefficient for different nanoparticle concentrations are shown in Fig. 4 for both straight and curved pipes.

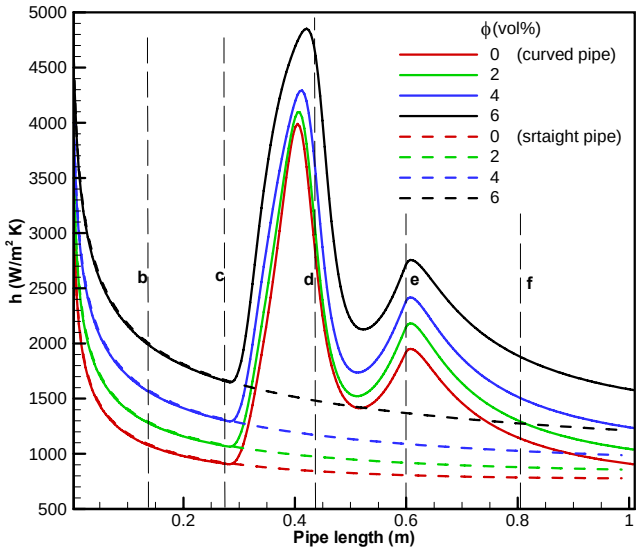

Figure 4. Axial variations of the heat transfer coefficient for different nanoparticle concentrations in straight and curved pipes at Re = 833.

The solid lines are related to the curved pipe, while the dashed lines are used for the straight pipe. The heat transfer coefficients are presented in dimensional form in accordance with the experimental data [15]. As expected, the heat transfer coefficients in the straight entrance section of the curved pipe (sections a - c) perfectly coincide with those of the straight pipe. However, along the bend, due to secondary flows superimposed on the axial flow field, strong fluid mixing occur, which leads to a more uniform cross sectional temperature distribution and reduces the peripheral averaged wall temperature as discussed later. Since the mean fluid temperatures in both cases are basically the same due to the constant applied heat flux as shown in Fig. 5, the heat transfer coefficients increase along the bend.

In Fig. 6, the axial variations of the peripheral averaged wall temperatures are shown for the same flow conditions as those of Fig. 4. As mentioned earlier, the averaged wall temperature decreases along the bend due to the secondary flows in the bend. Therefore, the temperature difference between the wall

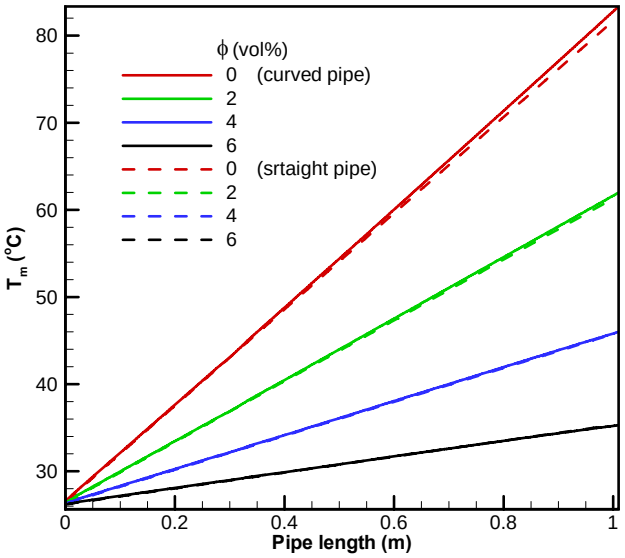

Figure 5. Axial variations of the cross sectional mean temperature for different nanoparticle concentrations and both geometries at Re = 833.

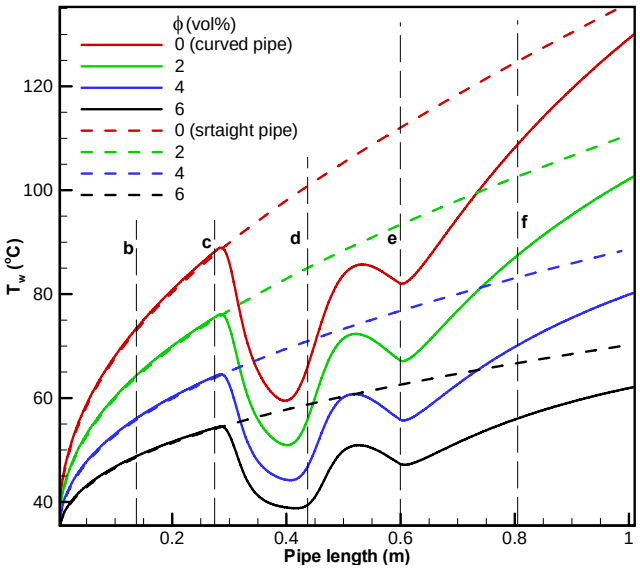

Figure 6. Axial variations of the peripherally averaged wall temperature for different nanoparticle concentrations in both geometries at Re = 833.

and the fluid bulk decreases, which leads to the increase in heat transfer rates observed in Fig. 4. The reduction in temperature difference is considerable at some axial locations; for example, for the based fluid and at the axial location of 0.4 m from the inlet, the temperature difference is about 33°C for the straight pipe and about 10°C for the curved pipe.

Figure 4 also shows that the heat transfer rates increase with increasing nanoparticle volume fraction. Figures 6 and 7 also indicate that both the averaged wall temperature and the cross sectional mean temperature decrease with increasing nanoparticle concentration. However, the decrease in the mean

temperature is larger as compared to the decrease in the averaged wall temperature, which leads to increased heat transfer rates.

Furthermore, from Fig. 4 it can be seen that the thermal entrance length increases as the nanoparticle volume fraction increases. This is more evident for the case of a straight pipe, which can be justified by the constant Reynolds number considered here and the increase in Prandtl number due to the increase in nanoparticle concentration.

The axial variations of the cross sectional mean temperature at Re = 833 and different nanoparticle concentrations are plotted in Fig. 5. All flow conditions are the same as those in Fig. 4. As indicated before, for a constant heat flux condition and the flow geometries considered here, the curved and straight pipe must have identical mean temperatures since the flow rates and pipe wall areas are the same. The slight discrepancies close to the exit region between the curved and straight pipes for the case of base fluid may be attributed to the fact that the straight part after the curved section is not long enough for the thermally fully developed conditions to be established at the exit of the curved pipe.

The linear axial variations of mean temperatures in Fig. 5 are because of the constant heat flux condition; however, the reductions in the mean temperatures due to the increase in nanoparticle concentrations are related to the increase in the Prandtl number; signaling that momentum diffusion occurs faster than heat diffusion. Therefore, the total temperature variation across the pipe decreases as the nanoparticle concentration is increased. In Table 1, the inlet and outlet temperature differences for different nanoparticle concentrations are listed for a curved pipe. This table indicates that a specified amount of heat transfer can be achieved with lower bulk and wall temperatures if the nanoparticle concentration is increased.

Table 1. Total outlet and inlet temperature differences for different nanoparticle concentrations in a curved pipe at Re=833.

ϕ (volume %)	ΔT (out - in)
0	55.9
2	35.3
4	19.7
6	9.2

In addition to the secondary flows in curved pipes, which reduce the wall temperature as compared to straight pipes, Fig. 6 also shows that increasing the nanoparticle concentration results in a lower wall temperature for both geometries. Since a higher nanoparticle concentration augments the effective conductivity with little change in density while reducing the heat capacity, the thermal diffusion in a nanofluid increases.

As mentioned earlier, the temperature profiles are more uniform in a curved pipe than in a straight pipe due to flow mixing as can be seen in Fig. 7. In this figure the temperature profiles in the symmetry plane of the exit section for different nanoparticle concentrations are shown for both geometries. Thus, for the constant wall heat flux case, heat spreads out through the fluid faster, causing the wall temperature to

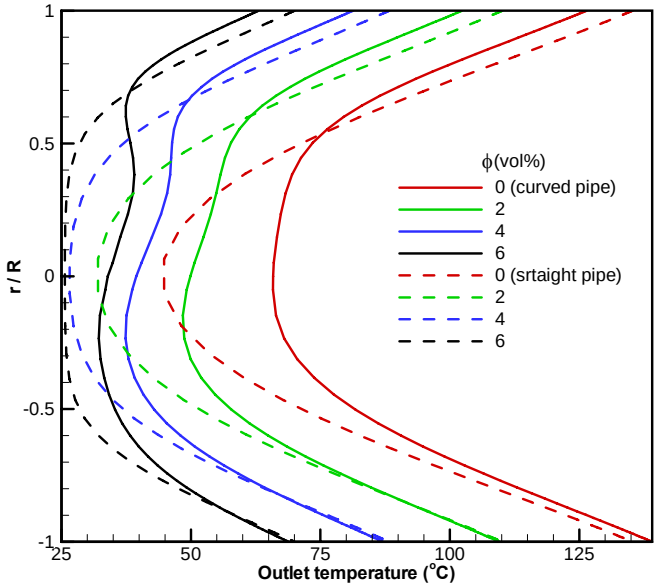

Figure 7. Temperature profiles in the symmetry plane of the exit section for different nanoparticle concentrations in both geometries at Re = 833.

decrease. Clearly, at higher nanoparticle concentrations, due to the increase in thermal diffusion, the temperature profiles become more uniform in both geometries.

The increase in heat transfer rates due to the curvature effects and nanofluids are accompanied by an undesirable effect which is an increase in pressure drop. In Table 2, the total pressure drops across the pipe for both geometries at different nanoparticle concentrations are listed. As expected, the pressure drops in a curved pipe are higher than those in a straight pipe. However, the pressure drop is very strongly influenced by the nanoparticle concentration such that, for a 6% concentration, the pressure drop increases by almost two orders of magnitude in both geometries. Table 2 also shows that the pressure drop due to curvature effects is relatively small as compared to nanoparticle effects.

Table 2. Total pressure drop for different nanoparticle concentrations in both geometries.

ϕ (volume %)	ΔP [Pa] (curved pipe)	ΔP [Pa] (straight pipe)
0	157	113
2	477	348
4	1847	1379
6	10016	7686

In general, the advantages of the nanofluids for cooling applications are directly related to the amount of the thermal conductivity increase leading to the heat transfer enhancement and to the amount of the viscosity increase leading to the higher pressure drop. Therefore, for cooling applications, the criterion for the choice of a nanofluid is that its thermal conductivity should increase more than its viscosity at higher nanoparticle concentrations. For the nanofluid used in the

present study, the viscosity of the based fluid increases faster than its thermal conductivity as the nanoparticle concentrations is increased at a given temperature. Therefore, the heat transfer enhancements come at the expense of considerable pressure drop. This criterion can also be explained in terms of the ratio of nanofluid Prandtl number (Pr_e) to the based fluid Prandtl number (Pr_f). It should be mentioned that this ratio is almost independent of temperature in the present case. In Table 3, the Prandtl number ratio is listed for different nanoparticle concentrations at 30^o C. The ratio increases considerably with the increase of nanoparticle concentration, which means viscosity increases faster than thermal conductivity at higher concentrations.

Table 3. The ratio of the nanofluid Prandtl number to the based fluid Prandtl number.

ϕ (volume %)	Pr_e / Pr_f
0	1
2	1.45
4	2.4
6	4.76

Nanofluids are particularly appealing in applications in which the relative importance of heat transfer enhancement to the pumping power is much higher such as in the thermal management of high-power electronics. Therefore, future research should be directed towards the selection of nanoparticle materials, shapes, and sizes such that the ratio of nanofluid Prandtl number to the based fluid Prandtl number becomes less than one.

CONCLUSION

Nanofluid heat transfer performance in straight and curved pipes of equal length and diameter has been studied numerically. A water/alumina nanofluid is modeled based on a single-phase approach, and the Navier-Stokes and energy equations for an incompressible Newtonian fluid are solved in a body-fitted coordinate system using a control-volume method. The temperature dependence of the thermophysical properties of the nanofluid is also considered. The accuracy of the model has been established by comparing the numerical results with available experimental data for nanofluid flows through straight pipes.

The results indicate that both the nanoparticle and curvature effects enhance heat transfer but at the expense of increased pressure drop. However, in the present case, the nanoparticle contribution to the pressure drop is dominant, which increases up to two orders of magnitude at higher nanoparticle concentrations. The ratio of the nanofluid Prandtl number to the based fluid Prandtl number is established as a parameter for the choice a nanofluid for a given application. This ratio must be less than 1 to achieve higher heat transfer rates together with acceptable pressure drops as the nanoparticle concentration is increased.

It is shown that for a given heat flux, lower outlet and inlet temperature differences are obtained by increasing the nanoparticle concentration. In other words, for a given inlet and outlet temperature difference, higher heat transfer rates can be achieved by adding nanoparticles. Both the curvature effects and the presence of nanoparticles result in more uniform cross sectional temperature profiles as well as lower peripherally averaged wall temperatures.

ACKNOWLEDGMENT

The financial support of the Ferdowsi University of Mashhad and the Natural Sciences and Engineering Research Council of Canada (NSERC) are gratefully acknowledged.

REFERENCES

[1] Das, S.K.., Choi, S.U.S., Yu, W. and Pradeep, T., 2008, *Nanofluids Science and Technology*, New Jersey, Wiley.

[2] Leong, K.C., Yang, C. and Murshed, S.M.S., 2006, "A model for the thermal conductivity of nanofluids – the effect of interfacial layer," Journal of Nanoparticle Research, **8**, pp. 245–254.

[3] Jang, S.P. and Choi, S.U.S. , 2007, "Effects of Various Parameters on Nanofluid Thermal Conductivity," ASME Journal of Heat Transfer, **129**, pp. 617-623.

[4] Chon, Ch.H., Kihm, K.D., Lee, Sh.P., Choi, S.U.S. , 2005, "Empirical correlation finding the role of temperature and particle size for nanofluid (Al2O3) thermal conductivity enhancement," Applied Physics Letters, **87**, pp. 1-3.

[5] Prasher, R., Bhattacharya, P., and Phelan, P.E., 2006, "Brownian-Motion-Based Convective-Conductive Model for the Effective Thermal Conductivity of Nanofluids," ASME Journal of Heat Transfer, **128**, pp. 588-595.

[6] Chopkar, M., Sudarshan, S., Das, P.K., and Manna, I., 2008, "Effect of Particle Size on Thermal Conductivity of Nanofluid," Metallurgical and Materials Transactions A, **39A**, pp. 1535-1542.

[7] Keblinski, P., Phillpot, S.R., and Choi, S.U.S., Eastman, J.A., 2002, "Mechanisms of heat flow in suspensions of nano-sized particles (nanofluids)," International Journal of Heat and Mass Transfer, **45**, pp. 855–863.

[8] Ding, Y., Alias, H., Wen, D., and Williams, R.A., 2006, "Heat transfer of aqueous suspensions of carbon nanotubes (CNT Nanofluids)", International Journal of Heat and Mass Transfer, **49**, pp.240-250.

[9] Xie, H., Wang, J., Xi, T., and Liu, Y., 2002, "Thermal Conductivity of Suspensions Containing Nanosized SiC Particles," International Journal of Thermophysics, **23**(2), pp. 571-580.

[10] Ding, Y., Alias, H., Wen, D., and Williams, R. A., 2006, "Heat Transfer of Aqueous of Carbon Nanotubes (CNT Nanofluids)," International Journal of Heat and Mass Transfer, **49**, pp. 240–250.

[11] Chen, H., Yang, W., He, Y., Ding, Y., Zhang, L., Tan, Ch., Lapkin, A.A., and Bavykin, D.V., 2008, "Heat transfer and flow behaviour of aqueous suspensions of titanate nanotubes (nanofluids)," Powder Technology, **183**, pp. 63–72.

[12] Anoop, K.B., Sundararajan, T., and Das, S. K., 2009, "Effect of particle size on the convective heat transfer in nanofluid in the developing region," International Journal of Heat and Mass Transfer, **52**, pp. 2189–2195.

[13] Godson, L., Raja, B., Mohan La, D., and Wongwises, S., 2010, "Enhancement of heat transfer using nanofluids-An overview," Renewable and Sustainable Energy Reviews, **14**, pp. 629–641.

[14] Williams, W.C., Buongiorno, J., and Hu, L.W., 2008, "Experimental investigation of turbulent convective heat transfer and pressure loss of alumina/water and zirconia/water nanoparticle colloids (nanofluids) in horizontal tubes," ASME Journal of Heat Transfer, **130** (042412), pp.1-6.

[15] Rea, U., McKrell, T., Hu, L., and Buongiorno, J., 2009, "Laminar convective heat transfer and viscous pressure loss of alumina–water and zirconia–water nanofluids," International Journal of Heat and Mass Transfer, **52**, pp. 2042–2048.

[16] He, Y., Mena, Y., Zhao, Y., Lu, H., and Ding, Y., 2009, "Numerical investigation into the convective heat transfer of TiO_2 nanofluids flowing through a straight tube under the laminar flow conditions," Applied Thermal Engineering, **29**, pp. 1965–1972.

[17] Akbarinia, A., and Laur, R., 2009, "Investigating the diameter of solid particles effects on a laminar nanofluid flow in a curved tube using a two

phase approach," International Journal of Heat and Fluid Flow, **30**, pp. 706–714.
[18] Haghshenas Fard M., Nasr Esfahany, M., Talaie, M.R., 2010, "Numerical study of convective heat transfer of nanofluids in a circular tube two-phase model versus single-phase model," International Communications in Heat and Mass Transfer, **37**, pp. 91–97.
[19] Lotfi, R., Saboohi, Y., and Rashidi, A.M., 2010, "Numerical study of forced convective heat transfer of Nanofluids-Comparison of different approaches," International Communications in Heat and Mass Transfer, **37**, pp. 74–78.
[20] Mokmeli, A., and Saffar-Avval, M., 2010, "Prediction of nanofluid convective heat transfer using the dispersion model," International Journal of Thermal Sciences, **49**, pp. 471–478.
[21] Akbarinia, A., 2008, "Impacts of nanofluid flow on skin friction factor and Nusselt number in curved tubes with constant mass flow," International Journal of Heat and Fluid Flow, **29**, pp. 229–241.
[22] Santra, A.K., Sen, S., and Chakraborty, N., 2009, "Study of heat transfer due to laminar flow of copper–water nanofluid through two isothermally heated parallel plates," International Journal of Thermal Sciences, **48**, pp. 391–400.
[23] He, Y., Men, Y., Liu, X., Lu, H., Chen, H., and Ding, Y., 2009, "Study on Forced Convective Heat Transfer of Non-Newtonian Nanofluids," Journal of Thermal Science, **18**(1), pp. 20−26.
[24] Naphon, P. and Wongwises, S., 2006, "A review of flow and heat transfer characteristics in curved tubes," Renewable and Sustainable Energy Reviews, **10** (5), pp. 463-490.
[25] Berger, S.A., Talbot, L., and Yao, L.S., 1990, "Flow in curved pipes," Annu. Rev. Fluid Mech., **15**, pp. 461–512.
[26] Kakac, S., Shah, R.K., and Aung, W., 1987, *Handbook of Single-Phase Convective Heat Transfer*, New York, Wiley, (Chapter 5).
[27] Van de Vosse, F.N., Van Steenhoven, A.A., Segal, A., and Janssen, J.D., 1989, "A Finite Element Analysis of the Steady Laminar Enterance Flow in a 90 Curved Tube," International Journal for Numerical Methods in Fluids, **9**, pp. 275-287.
[28] Dwyer, H. A., Cheer, A.Y., Rutaginira, T., and Shahcheraghi, N., 2001, "Calculation of Unsteady Flows in Curved Pipes," ASME Journal of Fluids Engineering, **123**, pp. 869–877.
[29] Chorin, A.J., 1968, "Numerical solution of the Navier-Stokes equations," Math. Comput., **22**, pp. 745-762.
[30] Dwyer, H.A., 1989, "Calculation of droplet dynamics in high temperature environments," Progress in Energy and Combustion Science, **15**, pp. 131-158.
[31] Renksizbulut, M., and Niazmand, H., 2006, "Laminar flow and heat transfer in the entrance region of trapezoidal channels with constant wall temperature," ASME Journal of Heat Transfer, **128**, pp. 63-74.